

**Origin of the fast magnetization tunneling in the single-molecule magnet
[Ni(hmp)(tBuEtOH)Cl]₄**

C. Kirman,^a J. Lawrence,^a S. Hill,^a E-C. Yang,^b and D. N. Hendrickson^b

^aDepartment of Physics, University of Florida, Gainesville, FL 32611

^bDepartment of Chemistry and Biochemistry, University of California at San Diego, La Jolla, CA 92093

We present high-frequency angle-dependent EPR data for crystals of [Ni_xZn_{1-x}(hmp)(t-BuEtOH)Cl]₄ ($x = 1$ and 0.02). The $x = 1$ complex behaves as a single-molecule magnet at low temperatures, displaying hysteresis and exceptionally fast magnetization tunneling. We show that this behavior is related to a 4th-order transverse crystal-field interaction, which produces a significant tunnel-splitting (~ 10 MHz) of the ground state of this $S = 4$ system. The magnitude of the 4th-order anisotropy, and the dominant axial term (D), can be related to the single-ion interactions (D_i and E_i) at the individual Ni^{II} sites, as determined for the $x = 0.02$ crystals.

Single-molecule magnets (SMMs) provide a molecular, or “bottom-up,” route to magnetic nanostructures [1]. They typically consist of a core of magnetically coupled transition metal ions, resulting in a well-defined giant spin ground state. Their main attraction is an intrinsic bistability, which is realized via a significant negative (easy-axis) magnetocrystalline anisotropy [see Eq. 1]. This bistability has aroused significant interest in terms of the use of SMMs in future molecular devices [2]. Unlike mesoscale magnetic particles of much larger dimensions, SMMs straddle the interface between classical and quantum behavior, displaying both superparamagnetic-like behavior, and magnetic quantum tunneling (MQT) at low temperatures. Furthermore, they offer all of the advantages of molecular chemistry, e.g. purity, solubility in various solvents, a well defined periphery of organic ligands, a crystalline assembly of monodisperse units, etc.. When grown as crystals, the magnetic unit is monodisperse—each molecule in the crystal has the same spin, orientation, magnetic anisotropy and structure, etc. [1]. Thus, bulk probes of SMM crystals enable fundamental studies of properties intrinsic to individual magnetic nanostructures.

We have recently synthesized a family of SMMs based on tetranuclear nickel clusters having the general formula $[\text{Ni}(\text{hmp})(\text{ROH})\text{X}]_4$, where $R = \text{CH}_3, \text{C}_2\text{H}_5$, etc., and $\text{X} = \text{Cl}$ or Br [3], and hmp^- is the monoanion of 2-hydroxymethylpyridine. Low-temperature ($\ll 1$ K) magnetization studies have demonstrated that each of these Ni_4 complexes exhibit MQT [3], albeit the temperature-independent MQT rate is exceptionally fast (too fast to measure). In this article, we focus on the $[\text{Ni}(\text{hmp})(\text{t-BuEtOH})\text{Cl}]_4$ member of this family, where t-BuEtOH is 3,3-dimethyl-1-butanol. Previous electron paramagnetic resonance (EPR) studies have confirmed the expected $S = 4$ ground state, as well as showing that it possesses an easy-axis-type anisotropy [3,4], i.e. a negative axial crystal-field parameter ($D \approx -0.600 \text{ cm}^{-1}$). Our motivation for studying the $R = \text{t-BuEtOH}$ complex stems partly from its high symmetry (S_4). More importantly,

however, crystals of this complex contain no solvate molecules. As recent studies of Mn_{12} -acetate have shown, solvent molecules can have a pronounced influence on the quantum properties of SMMs [5,6]. The Ni_4 SMMs offer no exception. EPR spectra for the $R = \text{CH}_3$ and C_2H_5 Ni_4 complexes consist of extremely broad absorption peaks, with multiple fine structures, making detailed analysis rather difficult [4]. In contrast, EPR spectra for the t-BuEtOH complex exhibit very sharp lines (see Fig. 1 and [4]).

The effective spin Hamiltonian for an isolated Ni_4 SMM is [1]:

$$\hat{H} = D\hat{S}_z^2 + g\mu_B\mathbf{B}\cdot\hat{\mathbf{S}} + \hat{O}_4 + \hat{H}'; \quad (1)$$

where $\hat{\mathbf{S}}$ is the spin angular momentum operator with components \hat{S}_x , \hat{S}_y , and \hat{S}_z ; g is the Landé g -factor and \mathbf{B} is the applied field strength; \hat{O}_4 denotes fourth-order crystal-field terms; and \hat{H}' describes additional perturbations such as hyperfine and intermolecular interactions [1-5]. MQT is caused by terms in the Hamiltonian which do not commute with the dominant $D\hat{S}_z^2$ interaction, e.g. terms containing \hat{S}_x and \hat{S}_y . The rhombic term, $E(\hat{S}_x^2 - \hat{S}_y^2)$, is symmetry forbidden. Thus, the leading term in the crystal-field that could cause MQT would be the fourth-order $B_4^4(\hat{S}_+^4 - \hat{S}_-^4)$ interaction. We note that this operator connects states differing in m_s (projection of S along z) by ± 4 in second order of perturbation theory. Consequently, it is quite effective at causing tunneling between the $m_s = \pm 4$ ground states. While its effects are rather weak at low fields, causing tunnel splittings of order 10 MHz (see below), the interaction becomes zeroth-order in the presence of a large transverse field ($g\mu_B B > DS$). In this way, angle-dependent hard-plane EPR experiments can be used to determine both the symmetry of the dominant transverse terms in Eq. 1 [5,6], and to quantify their magnitudes (note: D and g are isotropic in the xy -plane). Similarly, angle-

dependent EPR studies of a doped $[\text{Ni}_x\text{Zn}_{1-x}(\text{hmp})(\text{t-BuEtOH})\text{Cl}]_4$ ($x = 0.02$) crystal enable a determination of the complete crystal-field tensor associated with each Ni^{II} site (D_i and E_i parameters, and associated Euler angles), which one can then relate to the full Ni_4 spin Hamiltonian [7].

High-frequency (40–300 GHz) single-crystal EPR measurements were carried out using a millimeter-wave vector network analyzer (MVNA) in combination with an over-moded cavity perturbation technique which we have described elsewhere [8]. In order to enable in-situ rotation of the sample relative to the applied magnetic field, we employed a split-pair magnet with a 7 T horizontal field and a vertical access. Smooth rotation of the entire rigid microwave probe, relative to the fixed field, was achieved via a room temperature stepper motor. Synthetic procedures for obtaining single crystals of $[\text{Ni}_x\text{Zn}_{1-x}(\text{hmp})(\text{t-BuEtOH})\text{Cl}]_4$ ($x = 1$ and 0.02) have been described previously [3]. For the angle-dependent measurements, pyramidal-shaped single-crystal samples [approximate dimensions: $1.5 \times 1.5 \text{ mm}^2$ square base; 2 mm height (see insets to figures)] were aligned by hand within a cylindrical cavity (dia. = 7.62 mm, length = 8.38 mm) for field rotations in the appropriate crystallographic plane. Small mis-alignments are easily corrected during data analysis (see below). In all cases, the temperature was stabilized relative to a calibrated CernoxTM resistance sensor using a combination of heaters and cold helium gas flow.

Figure 1(a) displays the microwave transmission through the cavity at a temperature of 10 K and a frequency of 101.2 GHz, for the $x = 1$ complex; in this experiment, the magnetic field was rotated in the hard $[xy \text{ or } (100)/(010)]$ plane of the crystal. The data in Fig. 1(a) correspond to the case where the field is applied 23° away from one of the edges of the square base of the pyramidal sample $[x \text{ or } y \text{ direction, see inset to (b)}]$, corresponding to the hard axis of the crystal ($\phi = 0$). The sharp minima in transmission correspond to EPR absorptions; these resonances have

been labeled according to the scheme described in Ref. [6]. The splitting of the highest field peak (also weakly visible in the 4.5 T peak) is caused by a weak disorder associated with the t-BuEtOH ligand which gives rise to micro-environments with slightly different D values (-0.600 cm^{-1} and -0.577 cm^{-1} [4]). This disorder, which sets in below a structural transition at 46 K, has been confirmed via specific heat and X-ray measurements [9].

Figure 1(b) displays a grayscale contour plot of the absorption intensity, as a function of the magnetic field strength and its orientation (ϕ) within the hard plane. Immediately apparent is the 4-fold behavior of the peak position shifts. The maxima occur when the field is along the hard directions ($\phi = 0^\circ, 90^\circ$, etc.). The minima correspond the medium axes, which are in between the hard directions ($\phi = 45^\circ, 135^\circ$, etc.). The hard directions ($\phi = 0^\circ, 90^\circ$, etc.) are located at -23° (or $+23^\circ$) and 67° (or -67°) away from the crystallographic (100) and (010) directions. The 4-fold line-shifts are caused by the fourth-order $B_4^4(\hat{S}_+^4 - \hat{S}_-^4)$ interaction in Eq. (1). Superimposed on the absorption maxima (darker regions) in Fig. 1(b) are fits (white curves) to the data. The 4-fold shifts are reproduced for all peaks (including $\beta 4'$) with just a single parameter, $B_4^4 = 4 \times 10^{-4} \text{ cm}^{-1}$. In addition, the hard-plane g -factors ($g_x = g_y = 2.23$) may be obtained from the average peak positions. The satellite peak ($\beta 4'$) between 3.15 T and 3.3 T, which is only seen for angles close to $\phi = 0^\circ$, is a double quantum transition [all others in Fig. 1b are $\Delta m_s = 1$]. This transition is only allowed when there is a significant microwave H_1 -field component parallel to the applied DC field H_0 . It turns out that the relative orientations of H_1 and H_0 vary upon rotation of the cavity such that they are approximately parallel for $\phi = 0^\circ$ and 180° , and perpendicular for $\phi = 90^\circ$ and 270° [10]. Spectra obtained at different ϕ angles were normalized to the intensity of $\alpha 4$, hence $\beta 4'$ vanishes in the vicinity of $\phi = 90^\circ$, i.e. the 2-fold nature of this peak is an instrumental artifact and not connected to any intrinsic 2-fold symmetry

of the sample. Finally, we note that the obtained large fourth-order B_4^4 term results in a 10 MHz tunnel splitting between the $m_s = \pm 4$ ground states, thus explaining the fast magnetization tunneling in this system.

Figure 2(a) displays a series of EPR spectra for a doped $[\text{Ni}_{0.02}\text{Zn}_{0.98}(\text{hmp})(\text{tBuEtOH})\text{Cl}]_4$ crystal at 2.5 K and 120 GHz. The field was rotated in the xz plane: in the top trace, the field is oriented at $\theta = -34^\circ$ away from the hard plane; successive traces were taken in 2.5° steps towards the hard plane. Fig. 2(b) displays the angle-dependence of the EPR peak positions for a full 360° rotation of the sample (inset depicts the experimental geometry). Due to the low concentration of Ni^{II} in the sample, we can assume that the EPR spectra are dominated by $\text{NiZn}_3(\text{hmp})_4(\text{tBuEtOH})_4\text{Cl}_4$ molecules having $S = 1$. However, the Ni^{II} ion can reside at four different sites on the molecule and, in general, the crystal-field tensor at each site will have a different orientation, albeit related by the symmetry group of the molecule. Indeed, this is the reason why one observes a pair of maxima either side of $\theta = 0^\circ$ and 180° in Fig. 2(b); these maxima would coincide at $\theta = 0^\circ$ and 180° if the Ni^{II} crystal-field tensors were collinear and coincident with the full Ni_4 crystal-field tensor. Thus, these experiments indicate that the Ni^{II} tensors are tilted with respect to the molecule. In fact, all of the peaks in Fig. 2 correspond to the same transition, as indicated in the $S = 1$ energy level diagram (inset to Fig. 2a). The four resonance branches originate from each of the four inequivalent Ni^{II} sites. For the ideal experimental geometry, one should expect the two high-field branches to lie on top of each other. However, a slight sample mis-alignment lifts this degeneracy. Nevertheless, this is taken into consideration in our fitting procedure. Similar experiments performed in a plane parallel to the diagonals of the pyramidal sample (inclined 45° to the data in Fig. 2), reveal that the Ni^{II} easy axes are tilted along the (100) and (010) directions, and inclined 15° away from the (001) direction. This likely explains why

the hard directions for the Ni₄ molecule are found between these directions (see Fig. 1), i.e. along (100) and (010).

Frequency-dependent studies (not shown) performed with the field along one of the high symmetry directions provide access to the crystal-field parameters for the Ni^{II} ions: $D_i = -5.27 \text{ cm}^{-1}$ and $E_i = -1.2 \text{ cm}^{-1}$. A simple calculation, which assumes no tilting, enables a comparison between D_i and the Ni₄ D value: the negative E value yields $D = -0.66 \text{ cm}^{-1}$; the positive E value yields $D = -0.69 \text{ cm}^{-1}$ [7]. Such agreement (within 10%) is impressive, considering the approximate nature of the calculation. Armed with Ni^{II} crystal field parameters, one can also fit the angle-dependent data for NiZn₃(hmp)₄(t-BuEtOH)₄Cl₄ for each plane of rotation [i.e. solid curves in Fig. 2(b)]. As discussed above, our fitting procedure allows for mis-alignments between the actual and assumed rotation planes; indeed, such a mis-alignment of about 8° is the reason for the asymmetry between the heights of the maxima in Fig. 2(b). A full account of this analysis will be presented elsewhere [7]. However, the easy axis tilting and significant E term associated with the Ni^{II} ions provide a natural explanation for the significant B_4^4 term and the fast magnetization relaxation for the Ni₄ system.

This work was supported by the National Science Foundation (DMR0103290 and DMR0239481). S.H. is a Cottrell scholar of the Research Corporation.

References cited

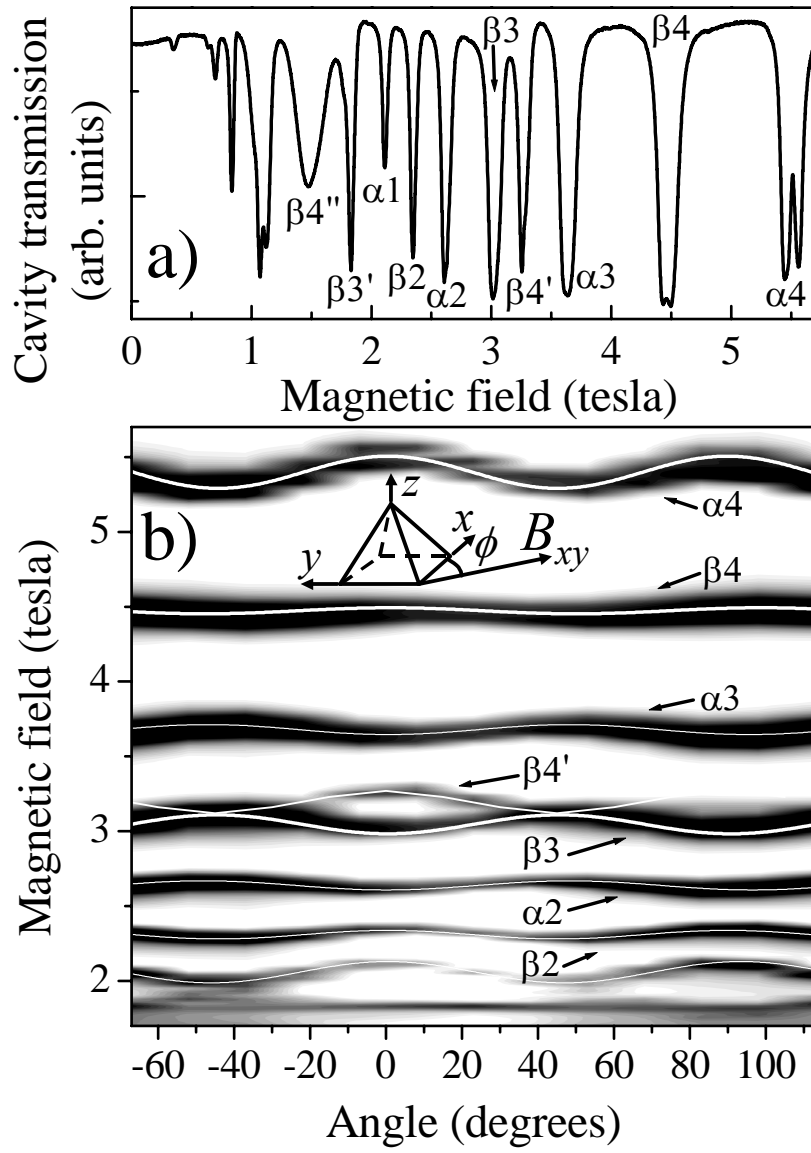
- [1] D. Gatteschi and R. Sessoli, *Angew. Chem.* **42**, 268 (2003).
- [2] S. Hill, R. S. Edwards, N. Aliaga-Alcalde, G. Christou, *Science* **302**, 1015 (2003).
- [3] E-C. Yang, W. Wernsdorfer, S. Hill, R. S. Edwards, M. Nakano, S. Maccagnano, L. N. Zakharov, A. L. Rheingold, G. Christou, D. N. Hendrickson, *Polyhedron* **22**, 1727 (2003).

- [4] R.S. Edwards, S. Maccagnano, E-C. Yang, S. Hill, W. Wernsdorfer, D. Hendrickson, and G. Christou, J. Appl. Phys. **93**, 7807-7809 (2003).
- [5] S. Hill, R. S. Edwards, S. I. Jones, J. M. North, N. S. Dalal, Phys. Rev. Lett. **90**, 217204 (2003).
- [6] S. Takahashi, R. S. Edwards, J. M. North, S. Hill and N. S. Dalal, Phys. Rev. B **70**, 094429 (2004).
- [7] E-C. Yang, C. Kirman, S. Hill and D. N. Hendrickson, Inorg. Chem. (available online, 2005).
- [8] M. Mola, S. Hill, P. Goy and M. Gross, Rev. Sci. Inst. **71**, 186 (2000).
- [9] E-C. Yang, J. Lawrence, S. Hill, C. Ramsey, N. S. Dalal, M. Olmstead, and D. N. Hendrickson (unpublished).
- [10] We note that, due to the relatively large size of the sample used in these studies, the microwave H_1 is not uniform over the sample. Therefore, there will always be weak components of H_1 both parallel and perpendicular to H_0 .

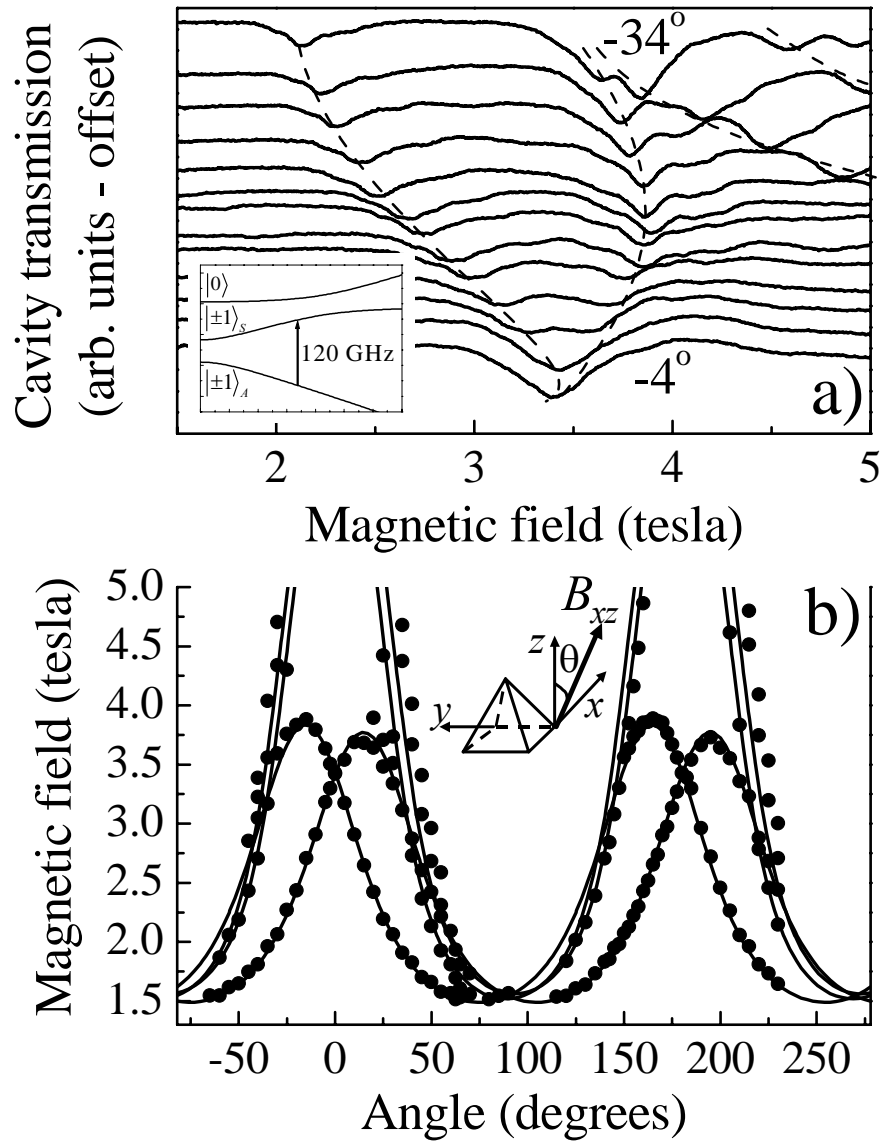
Figure captions

Fig. 1(a) Transmission through the cavity containing a $[\text{Ni}(\text{hmp})(\text{t-BuEtOH})\text{Cl}]_4$ single-crystal at 10 K and 101.2 GHz; the field is applied 23° away from one of the edges of the square base of the pyramidal sample [x or y direction, see inset to (b)]. The resonances have been labeled according to the scheme described in ref. [6]; the primed peaks (e.g. β_4') represent double quantum transitions; and β_4'' originates from the downward sloping branch of β_4 in the frequency versus field plot, i.e. β_4 is seen at two field positions (see Fig. 1 of ref. [6]). (b) Grayscale contour plot of the absorption intensity in (a), as a function of the magnetic field strength and its orientation (ϕ) within the hard plane; the white curves are fits to the data (see main text for details).

Fig. 2(a) EPR spectra for a doped $[\text{Ni}_{0.02}\text{Zn}_{0.98}(\text{hmp})(\text{t-BuEtOH})\text{Cl}]_4$ crystal at 2.5 K and 120 GHz. The field was rotated in the xz plane: in the top trace, the field is oriented at $\theta = -34^\circ$ away from the hard plane; successive traces were taken in 2.5° steps towards the hard plane. The inset shows the energy versus magnetic field (Zeeman) diagram for $S = 1$, for a field tilted 15° away from the easy axis; the levels are labeled in zero magnetic field ($|\pm 1\rangle_S$ and $|\pm 1\rangle_A$ correspond to symmetric and antisymmetric combinations of the $S = \pm 1$ states) and the arrow indicates the origin of the EPR transitions seen in the main figure. (b) Angle-dependence of the EPR peak positions in (a) for a full 360° rotation of the sample (inset depicts the experimental geometry); the solid curves are fits to the data.



Kirman et al., Fig. 1



Kirman et al., Fig. 2